Available online at www.sciencedirect.com
ScienceDirect
Proceedings of the Combustion Institute 33 (2011) 3367–3374
Proceedings of the Combustion Institute
www.elsevier.com/locate/proci

An aerosol rapid compression machine for studying energetic-nanoparticle-enhanced combustion of liquid fuels

Casey Allen [a], Gaurav Mittal [b], Chih-Jen Sung [c], Elisa Toulson [a], Tonghun Lee [a,*]

[a] Department of Mechanical Engineering, Michigan State University, East Lansing, MI 48824, USA
[b] Department of Mechanical Engineering, University of Akron, Akron, OH 44325, USA
[c] Department of Mechanical Engineering, University of Connecticut, Storrs, CT 06269, USA

Available online 6 August 2010

Abstract

The use of energetic nanoparticles offers a promising means of adjusting the reactivity of liquid fuels for enhanced combustion stability in next generation propulsion systems. This work outlines the development of a novel aerosol rapid compression machine (RCM) for studying the impact of energetic nanoparticles on reducing the ignition delay of liquid fuels, and a proof-of-concept demonstration is presented using ethanol and JP-8. Fuel droplets are generated using an ultrasonic nozzle. The seeding of 50 nm aluminum nanoparticles in the liquid fuel is achieved by using a combination of chemical surfactants in addition to mixing in an ultrasonic bath. The autoignition delay is measured for neat and nanoparticle-enhanced mixtures at compressed conditions of 772–830 K and 12–28 bar in the RCM. The results show that significant changes in the ignition delay can be observed using a low concentration (2%-weight) of energetic nanoparticles. For ethanol and JP-8, ignition delays were reduced by 32% and 50%, respectively. Measurements to verify the uniformity of aerosol dispersion in the RCM, the reproducibility of the RCM data, and a method for approximating compressed temperature are also presented.

Keywords: Autoignition; Energetically-enhanced combustion; Nanoparticle; Ethanol; JP-8

1. Introduction

The next generation of advanced propulsion systems will strive to combine dramatically enhanced power output with high efficiency and control; pushing combustion to occur at the very limits of flammability and stability for a specific fuel. To address the potential challenges ahead in terms of achieving combustion stability, advanced technologies for active combustion enhancement such as high-energy laser spark ignition [1], turbulent jet ignition [2], and plasma jet ignition [3] are being investigated for a range of novel concept engines. The problem is further compounded by the introduction of new and alternative fuel blends which can exhibit drastic variation in combustion

* Corresponding author. Address: Department of Mechanical Engineering, Michigan State University, 2555 Engineering Building, East Lansing, MI 48824, USA. Fax: +1 517 432 3341.
E-mail address: tonghun@msu.edu (T. Lee).

1540-7489/$ - see front matter © 2010 The Combustion Institute. Published by Elsevier Inc. All rights reserved.
doi:10.1016/j.proci.2010.06.007

characteristics depending on the operational conditions. A new strategy to address this issue is to change the reactivity and the energetic output of the fuel itself by adding highly exothermic, energetic nanoparticles to the liquid fuel.

Energetic nanoparticles are nano-sized (10−100 nm range) particles, usually metallic with a passivated oxide layer, and are characterized by a high rate of energy release [4]. Energetic nanoparticles offer a high volumetric heat of oxidation, enabling transportation of more energy per given fuel volume. When mixed in a fuel or a composite, they generally exhibit faster ignition timescales due to the dramatic increase in the surface-to-volume ratio [5], and can ignite below the bulk melting point of the metal due to rapid temperature gradients through their thin oxide layers [6]. Nano-sized energetic particles offer the potential of controlled reactivity of the fuel, increased combustion efficiencies, and increased safety in handling.

The purpose of this study is to develop an aerosol rapid compression machine (RCM), a flexible experimental platform to investigate the ignition characteristics of liquid fuels where energetic nanoparticles are suspended by surfactants. Charging the RCM with an aerosol instead of vaporized fuel is important as the embedded nanoparticles must also be carried into the combustion chamber and cannot undergo vaporization. The new testbed is designed for combustion at practical high-pressure conditions and provides optical access for laser and optical diagnostics to be added in the future. As a proof-of-concept demonstration of the aerosol RCM's functionality, energetic-nanoparticle-enhanced combustion of ethanol and JP-8 will be presented.

2. Target fuels for demonstration

The target fuels used in the demonstrations are ethanol and JP-8 with 50 nm average particle size (APS) aluminum nanoparticles. Ethanol was chosen primarily because the combustion characteristics are well-defined and a detailed chemical kinetic mechanism [7] is available. Also, ethanol is an easy fuel to handle and adequate for initial testing of the aerosol RCM. Therefore, most of the characterization of the aerosol RCM was conducted using ethanol.

Aluminum nanoparticles were selected because they have a high heat of oxidation and have received much attention in the literature [8,9]. Compared to the ignition temperatures of micron-sized particles (1300−2100 K) [10,11], aluminum nanoparticles have shown ignition well below the bulk melting temperature [11] and as low as 800 K [12], enhancing the burning rate of propellants by 10–20 times over conventional bulk aluminum particles [5]. Their ignition profiles are generally very rapid and recently have shown potential as additives for liquid fuels [13,14]. For this study, we are using 50 nm Alex® particles from Argonide Corporation, which are suspended in both ethanol and JP-8.

To extend the demonstration of the aerosol RCM to practical fuels, measurements of energetic-nanoparticle-enhanced ignition are also shown using JP-8, the most widely used jet fuel for the Air Force and the candidate for the 'single fuel forward' policy of the Army. A number of studies have looked into the thermal oxidation chemistry of JP-8 including ignition delay measurements in shock tubes and RCM [15–17], chemical kinetics and emission studies in experimental burners [18], and numerical modeling of both reduced and detailed chemical kinetic mechanisms for surrogate blends of JP-8 [19,20]. These studies have found large variations in the ignition properties of JP-8 as a function of initial conditions which can be problematic for design of novel propulsion systems, and where nanoparticles can be of benefit by tuning the reactivity.

3. Experimental testbed: aerosol rapid compression machine

3.1. Design of aerosol rapid compression machine (RCM)

Central to this study is the design and construction of an aerosol RCM for controlled investigation of energetically-enhanced ignition of fuels. An RCM uses the mechanical stroke of a piston to generate high temperatures and pressures for combustion, and many types are available, with variations in mechanisms for rapid acceleration and deceleration of the piston [21–24]. The ability to charge fuels as droplets is a unique feature of the aerosol RCM and a necessary function for this study since (1) many heavy fuels are difficult to vaporize, (2) droplets represent more realistic engine conditions, and (3) nanoparticle-enhanced fuels cannot be vaporized altogether. A similar concept has been previously applied in a shock tube at Stanford University [13] for testing nanoparticle slurries for chemical rocket propulsion. In comparison to a shock tube, an RCM can offer longer test times, realistic fuel concentrations, and the ability to carry out multiple test runs within a short time period. The issues of longer compression times and heat loss in an RCM are of minimal impact here as our goals are to understand the general characteristics of new ignition concepts and not detailed chemical kinetics.

The aerosol RCM, illustrated in Fig. 1, is pneumatically-driven and hydraulically-stopped by an optimized pin-and-groove mechanism [23]. The core of the machine is modeled after the design of Mittal and Sung [23] which utilizes a 5-in.

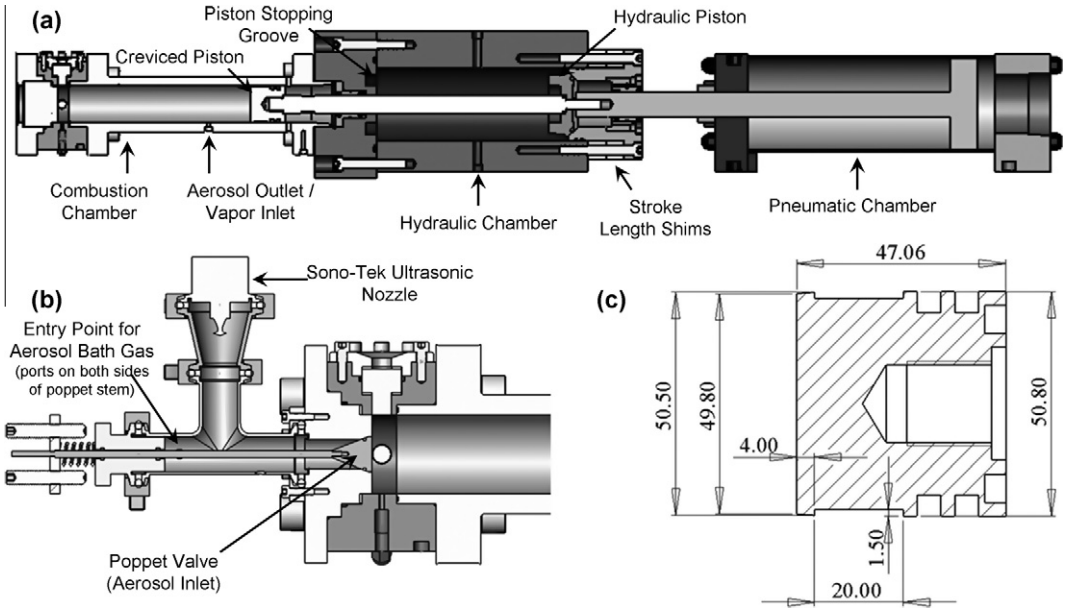

Fig. 1. RCM schematics. (a) Overall RCM schematic depicting combustion chamber, hydraulic chamber and pneumatic chamber; (b) aerosol unit that may replace end window and flange in overall setup; (c) creviced piston with dimensions (in millimeters) [23].

diameter pneumatic driving cylinder and a 2-in. diameter stainless steel combustion chamber. To promote the formation of an adiabatically-compressed core of gas, the RCM employs a creviced piston based on the CFD-optimized design of Mittal and Sung [23].

The RCM can accept an all vapor-phase charge of fuel, oxidizer and diluent, or the end window and flange may be replaced with a poppet valve assembly, as depicted in Fig. 1b, to facilitate an aerosol test. During an aerosol test, liquid fuel droplets are carried past the poppet valve into the combustion chamber by a continuous flow of oxidizer and diluent gases. The design of the poppet valve is intended to maximize mixture uniformity, and was developed by using computational fluid dynamics modeling (CFD) [25]. A Sono-Tek ultrasonic nozzle is used to generate the aerosol which is directed toward the poppet valve by a flow of incoming air. The nozzle is capable of producing aerosols with a median diameter of 18 μm, and the flow rate of the fuel is controlled using a syringe pump.

3.2. Aerosol discharge unit optimization

In an RCM ignition test, establishing a uniform charge is of critical importance for taking accurate, repeatable measurements. In a vapor test, the test charge is allowed to homogenize in the combustion chamber before compression begins. In an aerosol test, a gas and aerosol flow moves through the combustion chamber until the inlet (poppet) and outlet valves are closed just prior to the start of compression. The location of these valves and the gas inlets are identified in Fig. 1. Establishment of a uniformly distributed aerosol charge relies on turbulent mixing of the gas and aerosol as the aerosol-laden gas flow moves past the poppet valve. Given this consideration, CFD analysis using STAR-CCM+ was carried out to compare the turbulent swirling generated by airflow through the valve opening. The intent of the model was to provide high-level guidance for the design of the poppet valve, and the presence of the aerosol was not considered for the simulations. A two-dimensional grid was generated for each poppet valve design with higher mesh density near the poppet valve. Grid independence was confirmed in tests with an increased mesh density. For the tested models, increasing the mesh density led to only modest changes in peak velocity ($<1\%$). The simulations employed the k-ε turbulence model and no-slip boundary conditions were specified on all walls. Steady-state solutions were achieved for each model using an inlet velocity of 0.33 m/s. The results of the simulations are summarized here, and the reader is directed to Allen and Lee [25] where additional simulation results are reported.

Preliminary analysis of the poppet valve system identified two key design variables that contributed strongly to swirling flow in the combustion chamber. Figure 2b depicts these dimensions as V_1 and V_2. Simulations were conducted for different combinations of V_1 and V_2 and the results were

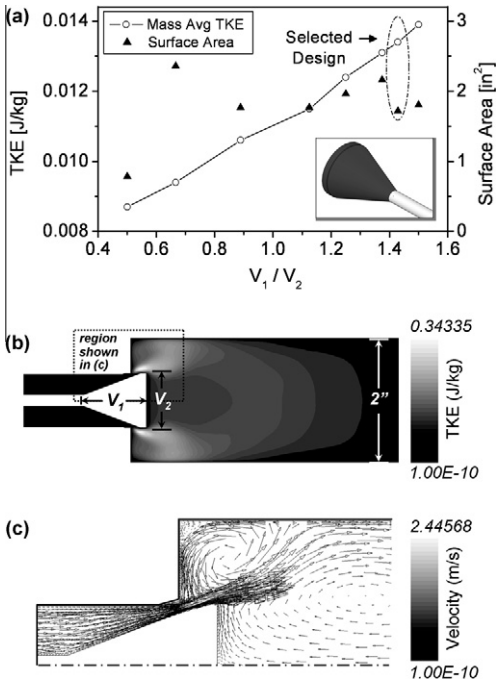

Fig. 2. CFD simulation results. (a) The mass averaged turbulent kinetic energy (TKE) and surface area for candidate poppet valve designs. The selected design ($V_1/V_2 = 1.429$) is highlighted. The inset image displays the poppet valve head and stem. The shaded area of the poppet head corresponds to the surface area used to compare valve designs. (b) The TKE field for the selected poppet valve design with description of region that is the focus of (c). (c) The velocity vectors for the selected poppet valve in the region described in (b).

evaluated using two design criteria: (1) the poppet valve should maximize turbulent swirl as measured by mass averaged turbulent kinetic energy (TKE); and (2) the poppet valve design should minimize the surface area where the impinging aerosol may settle out of the flow. The surface area we considered corresponds to the posterior side of the poppet valve, represented by the shaded surface of the inset poppet valve image in Fig. 2a. The TKE provided a scalar quantity to measure the relative strength of eddies in the flow and was used as a basis to compare turbulent swirl for different poppet valve designs. Figure 2a summarizes the TKE values for an array of V_1/V_2 values, each with a poppet valve opening distance of 0.25 in. Additional simulations with changes to the opening distance exhibited the same trend shown in Fig. 2a, of increasing mass averaged TKE values with increases in V_1/V_2. The optimum opening distance was determined experimentally through a light scattering experiment that is subsequently described. The simulations led to selection of the poppet valve design with $V_1/V_2 = 1.429$. This model is marked in Fig. 2a, and it can be seen the model has a comparatively large TKE value (0.0134 J/kg) and a relative minimum for surface area (1.718 in^2). Figure 2b displays the TKE field near the poppet valve for the selected design, and the figure describes the region which is the focus of Fig. 2c. Figure 2c displays the velocity vectors near the poppet valve for the selected design. The flow field clearly depicts the swirling motion generated as the flow emerges from the poppet valve. The steady-state solution cannot capture the inherently unsteady nature of the turbulence and vortex shedding; however, the models are sufficient when comparing relative swirling motion as a design criterion for the poppet valve. Compared to other models, the selected design showed higher TKE intensity near the poppet valve, and the TKE field values approached zero over a longer distance from the poppet valve.

The CFD simulations identified the poppet valve design for maximizing turbulence in the combustion chamber, but gave no direct indication of the overall aerosol distribution uniformity in the combustion chamber or the optimized poppet opening distance. We qualitatively addressed these questions by directing a laser light sheet (8 mW He–Ne) through an aerosol flow and imaging the light scattered by the aerosol droplets for three different opening distances: 1/8″, 3/16″ and 1/4″. The poppet valve assembly was attached to a glass tube for optical access, and the light sheet was directed vertically through the center plane of the glass tube. All of the tests were conducted with aerosol flow rates 0.15 kg/h and air flow rates of 10 SCFH, corresponding to a flow velocity of 0.28 m/s.

Figure 3 shows one representative image for each of the opening distances tested. The image for the 1/4″ opening distance clearly shows the aerosol droplets are entrained in the turbulent eddies, but the droplets are not uniformly distributed in the plane. By reducing the opening distance to 3/16″, we observed light scattering from a large portion of the imaged plane, indicating a more uniform distribution of aerosol in the chamber. Reducing the opening to 1/8″ also showed light scattering from a larger portion of the imaged plane when compared to the 1/4″ opening distance. However, the scattered light intensity decreased for the 1/8″ opening distance when compared to a 3/16″ opening. We suspect this occurs because more aerosol droplets settle on the back of the poppet valve for the 1/8″ opening distance thus reducing the aerosol loading in the chamber. The tests determined that a 3/16″ opening distance maximized droplet loading and uniformity of aerosol distribution. Based on this conclusion, all aerosol ignition tests in the RCM were performed with a 3/16″ poppet opening distance. Tests to quantify aerosol loading in the chamber have been carried out separately.

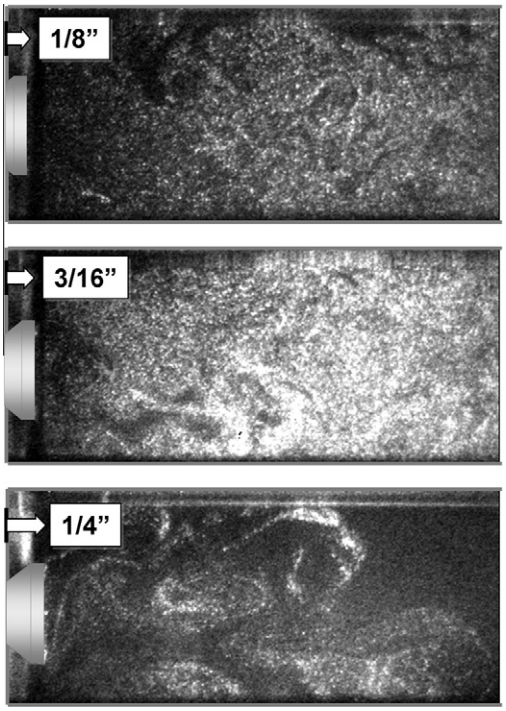

Fig. 3. Aerosol spatial distribution characterization. ICCD camera images of laser light scattered from aerosol droplets in glass tube. One representative image appears for each poppet valve opening distance.

4. Experimental overview

4.1. RCM operation protocol

To prepare the RCM for a new aerosol test, the combustion chamber is cleaned by opening the outlet (solenoid) and vacuuming the chamber to a pressure of <1 Torr. The inlet (poppet) valve is subsequently opened to introduce a steady flow of oxidizer and diluent to the combustion chamber. The desired initial pressure is established by adjusting a valve that exits to the vacuum pump. Once the pressure stabilizes (typically <3 min), the nozzle is activated and the syringe pump begins delivering liquid fuel to the nozzle. The syringe pump flow rate and filling time are calculated for the desired aerosol loading. After the filling period, the nozzle is deactivated while simultaneously closing the inlet and outlet valves. To minimize settling of the aerosol, the compression process is initiated immediately afterward (0.5 s) by opening a solenoid valve to relieve the hydraulic pressure. The pressure in the oil drops nearly instantaneously to atmospheric conditions, and is no longer sufficient to restrain the pressure behind the pneumatic piston. The piston lunges forward to compress the charge, leading to an increase in temperature and pressure.

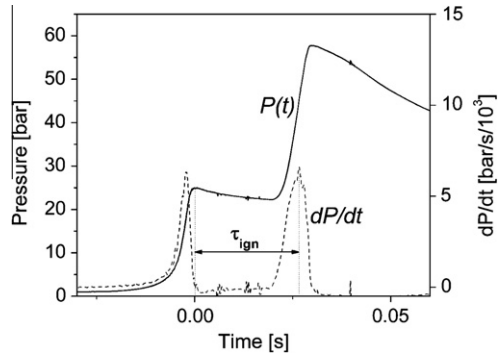

Fig. 4. Ignition delay definition. Reactive ethanol/air aerosol pressure trace [$P(t)$] and corresponding time derivative (dP/dt) used to calculate the ignition delay (τ_{ign}). Molar composition: $C_2H_5OH/O_2/N_2 = 1.0/6.0/22.6$. Conditions: $P_0 = 1$ bar, $T_0 = 343$ K, compression ratio = 14.2.

4.2. Experimental repeatability

Pressure measurements were taken during the ignition of neat ethanol aerosols to test the experimental repeatability of the RCM data. The measurements were taken using a Kistler 6125B pressure transducer, and the data were used to calculate the ignition delay (τ_{ign}), which we define as the time interval between the end of compression (top dead center, TDC) and the time at which the maximum rate of pressure rise due to ignition occurs [$(dP/dt)_{max}$]. TDC is identified as the time at which dP/dt becomes negative. Figure 4 illustrates this definition of ignition delay using data from a reactive ethanol aerosol test. Noise in the pressure trace is filtered while calculating the time derivative of pressure to aid in the consistent identification of the maximum compression pressure that corresponds to the arrival of the piston at TDC.

The operation protocol described in the previous section was used to investigate the experimental repeatability of ignition delays for a neat ethanol aerosol charge. Ignition tests were conducted under identical conditions (initial wall temperature: $T_0 = 338$ K; initial pressure: $P_0 = 1$ bar; compressed temperature: $T_c \approx 830$ K; compressed pressure: $P_c = 28$ bar) with a molar composition of $1.0\ C_2H_5OH + 6.0\ O_2 + 22.6\ N_2$, and the results shown in Fig. 5 support the repeatability of test data in the aerosol RCM. The figure shows six pressure traces that overlap identically during compression, and follow nearly the same profile during ignition. For the pressure traces shown in Fig. 5, the ignition delay is repeatable to within ±10%.

4.3. Temperature analysis

Calculation of the compressed temperature for an aerosol charge is complicated due to heat and mass transfer between the gas mixture and vaporiz-

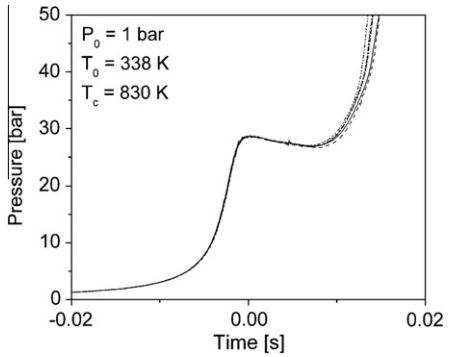

Fig. 5. Experimental repeatability. Demonstration of the experimental repeatability of autoignition of an ethanol aerosol charge at $P_c = 28$ bar, $T_c \approx 830$. Molar composition (aerosol test): $C_2H_5OH/O_2/N_2 = 1.0/6.0/22.6$. Initial conditions: $P_0 = 1$ bar, $T_0 = 338$ K.

ing aerosols. Although heat loss to the reaction chamber walls can be modeled through the effective volume approach commonly used in RCM studies [23,26], the volumetric heat transfer to the droplets that occurs during compression cannot be accurately characterized without the knowledge of aerosol vaporization history, e.g., measured by optical diagnostics. As a first step, here we calculate the compressed gas temperature under two limiting conditions. The upper bound of compressed temperature assumes no aerosol evaporation ('frozen aerosol'), while the lower bound of compressed temperature is calculated assuming complete evaporation before the onset of compression. Both limiting calculations proceed through the direct application of the effective volume approach, which assumes the existence of an adiabatically-compressed core of gases whose temperature is calculated as

$$\int_{T_0}^{T_c} \frac{\gamma}{\gamma - 1} \frac{dT}{T} = \ln \frac{P_c}{P_0} \tag{1}$$

where γ is the temperature-dependent specific heat of the gas mixture. Subscript 0 represents initial conditions while subscript c represents compressed conditions (at TDC). The actual T_c is expected to be bounded by the two limiting values, and would be closer to the lower bound value for highly volatile fuels. In the following, the T_c estimates presented are averages of the upper and lower bounds, and the uncertainties for these calculations approach ±40 K. Although the presence of the aerosol prevents formation of an adiabatic core for which Eq. (1) is intended, our approach provides an approximate T_c that is useful for understanding the temperature regime of nanoparticle-enhancement presented in this paper. Future studies will be devoted to the application of laser and optical diagnostics for improving the accuracy of these estimates.

4.4. Test mixture preparation

Tests investigating the influence of nanoparticles on the ignition of liquid fuel droplets used 50 nm APS aluminum nanoparticles from Argonide Corporation. All nanoparticle-enhanced tests used 2%-wt nano-aluminum in the respective liquid fuel where it was suspended by adding 0.03%-wt alizarin and 0.004%-volume triethanolamine before placing the solution in an ultrasonic bath for 120 min.

5. Results and discussion

Ignition delay measurements were taken for neat ethanol and compared with ethanol seeded with 2%-wt aluminum nanoparticles to investigate energetic-nanoparticle-enhanced combustion of our model system. A TEM image of the aluminum nanoparticles appears in the inset of Fig. 6. The TEM image shows the polydisperse nature of the nanoparticle size, and confirms the 50 nm APS technical specification of the nanoparticles. As a baseline for comparison, Fig. 6 shows the same neat ethanol pressure traces displayed in Fig. 5 from the repeatability experiment. Figure 6 also shows five pressure traces obtained for energetic-nanoparticle-enhanced ethanol combustion. It is evident from the pressure traces that the presence of the energetic nanoparticles leads to a significant reduction in the ignition delay time of ethanol. For the conditions tested ($P_c = 28$ bar, $T_c \approx 820$ K), the nanoparticles led to an average ignition delay reduction of 32% (4.6 ms) as compared to neat ethanol ignition delay times, and the results were reproducible to within ±20%. We emphasize that all of the neat ethanol and nanoparticle-seeded eth-

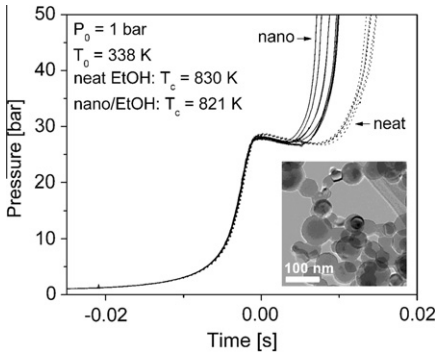

Fig. 6. Nanoparticle-enhanced ignition of ethanol. Reactive pressure traces for neat ethanol (dashed lines) and for 2%-wt nanoparticle-enhanced ethanol (solid lines). Inset displays TEM image of 50 nm APS aluminum nanoparticles. Molar composition for neat and nano-enhanced tests (aerosol + gas): $C_2H_5OH/O_2/N_2 = 1.0/6.0/22.6$.

anol tests were conducted with identical initial and operating conditions. Thus, in spite of the uncertainty in the T_c calculations our observation of a reduced ignition delay under these conditions supports the enhancement effect of the nanoparticles.

The energetic enhancement requires a lower concentration (2%-wt) than previously reported results for nanoparticle-enhanced liquid fuels which have used concentrations of $\geqslant$5%-wt nano-aluminum in *n*-dodecane to achieve ignition delay reductions of 40–75% in a shock tube at reflected temperatures of 1175–1249 K [13]. The results demonstrate the ability to energetically-enhance combustion through low concentrations of nanoparticles. The mechanism whereby aluminum nanoparticles reduce the ignition delay is not evident from this study, however, we hypothesize the ignition delay reduction is a result of an increased droplet thermal conductivity that has been observed in liquids seeded with nanoparticles (nanofluids) as compared to the thermal conductivity of the neat liquid [27]. We hypothesize that by adding aluminum nanoparticles to our liquid fuel, the thermal conductivity of the droplets increases which leads to more rapid internal heating and evaporation of the aerosol droplets, and thereby the earlier onset of fuel vapor ignition. Once the nanoparticle-carrying aerosol droplets evaporate, the nanoparticles are exposed to a hot, oxidizing environment, and the nanoparticles may ignite in advance of the fuel vapors, providing another route to a shorter ignition delay. Aluminum nanoparticles have been shown to ignite at temperatures as low as ~800 K [12], which are attained in our RCM experiments.

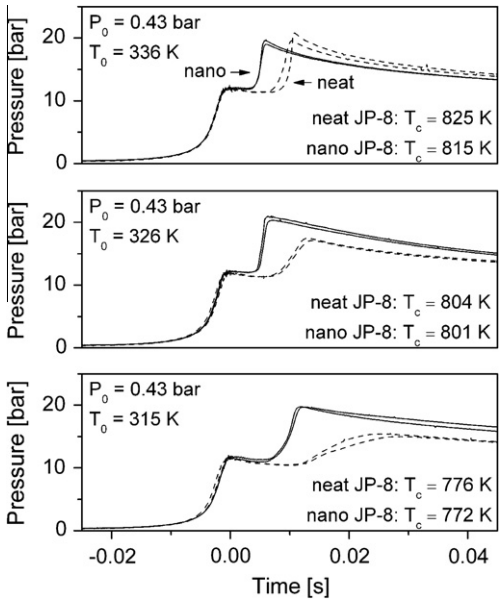

Fig. 7. Nanoparticle-enhanced ignition of JP-8. Reactive pressure traces for neat JP-8 (dashed lines) and for nanoparticle-enhanced JP-8 (solid lines). Molar composition: JP-8/O_2/N_2 = 1.0/32.5/122.2.

Energetic-nanoparticle-enhanced combustion was also tested by adding nano-aluminum (2%-wt) to JP-8. For all tests, we have assumed the molecular formula of JP-8 to be $C_{11}H_{21}$ [17]. Before testing nanoparticle-enhanced mixtures, we established a baseline for JP-8 by obtaining ignition delays for varying compressed temperatures. These compressed temperatures were calculated using Jet-A thermodynamic data [28] because JP-8 data is unavailable. Changes in compressed temperature were made by altering the initial temperature of the charge. Nanoparticle-enhanced mixtures of JP-8 were tested at the same conditions as the neat JP-8 fuel, and the results are shown in Fig. 7. The three plots in Fig. 7 compare neat JP-8 and nanoparticle-enhanced JP-8 ignition at three different compressed temperatures. For each of the compressed temperatures tested, the presence of the nanoparticles at 2%-wt concentrations led to a reduction in ignition delay of nearly 50%. Additionally, for all tests conducted at $T_c \leqslant 804$ K, the heat release rate is increased over that of the neat JP-8 test. To our knowledge, this is the first observation of nanoparticle-enhanced combustion of JP-8 at concentrations of less than 5%-wt. As with tests of nanoparticle-enhanced ethanol, we suspect the enhancement is a consequence of the increased thermal conductivity and faster evaporation of the liquid fuel and nanoparticle mixtures, relative to the neat liquid fuels.

6. Conclusion

An aerosol RCM has been designed and built for the purpose of testing nanoparticle-enhanced liquid fuels. The aerosol RCM has been demonstrated as a viable tool for investigating the influence of nanoparticle additives on the ignition delays of fuels. The poppet valve has been optimized to ensure consistent, reproducible results. Aerosol ignition tests confirmed that the RCM produces repeatable ignition delays within ±10% for identical test conditions.

The addition of energetic nanoparticles at low concentrations has been shown to significantly alter the ignition characteristics of ethanol and of JP-8. In ethanol, nano-aluminum concentrations as low as 2%-wt led to an average ignition delay reduction of 32% at the conditions tested. Nanoparticle-enhanced (2%-wt) JP-8 showed ignition delay reductions approaching 50% for all compressed temperatures tested, and led to faster heat release during ignition at compressed temperatures of less than 804 K. It is hypothesized that the addition of aluminum nanoparticles to the liquid fuel increases the thermal conductivity of the droplets relative to the neat liquid fuel droplets, and that this increased thermal conductivity

drives faster evaporation and the earlier onset of ignition. It is unclear whether the reduction in ignition delay results from fuel vapor ignition or from ignition of the nanoparticles. Ongoing work in our lab seeks to identify the contributions of these sources to the ignition delay reduction and to validate our hypothesis of faster evaporation.

Acknowledgements

We express our gratitude to the Michigan State University Foundation and to the U.S. Department of Energy for funding the construction of the RCM (Award #: DE-FC26-07NT43278). G.M. acknowledges and thanks the College of Engineering at the University of Akron for support of his work. C.J.S. was supported as part of the Combustion Energy Frontier Research Center, an Energy Frontier Research Center funded by the U.S. Department of Energy, Office of Science, Office of Basic Energy Sciences (Award #: DE-SC0001198).

References

[1] D. Bradley, C.G.W. Sheppard, I.M. Suardjaja, R. Woolley, *Combust. Flame* 138 (1–2) (2004) 55–77.
[2] E. Toulson, H.C. Watson, W.P. Attard, SAE 2009-01-0506 (2009).
[3] S.M. Starikovskaia, *J. Phys. D Appl. Phys.* 39 (16) (2006) R265–R299.
[4] K.K. Kuo, G.A. Risha, B.J. Evans, E. Boyer, in: *Materials Research Society Fall Meeting*, 2003, Paper No. AA1.1.
[5] G.V. Ivanov, F. Tepper, in: K.K. Kuo, T.B. Brill, R.A. Pesce-Rodriguez, et al. (Eds.), *Challenges in Propellants and Combustion: 100 Years After Nobel*, Begell House, New York, 1997, pp. 636–645.
[6] A. Rai, K. Park, L. Zhou, M.R. Zachariah, *Combust. Theor. Model.* 10 (5) (2006) 843–859.
[7] N.M. Marinov, *Int. J. Chem. Kinet.* 31 (3) (1999) 183–220.
[8] T. Bazyn, H. Krier, N. Glumac, *Combust. Flame* 145 (4) (2006) 703–713.
[9] M.W. Beckstead, Y. Liang, K.V. Pudduppakkam, *Combust. Explo. Shock Waves* 41 (6) (2005) 622–638.
[10] A.L. Breiter, V.M. Mal'tsev, E.I. Popov, *Combust. Expl. Shock Waves (English Translation of Fizika Goreniya i Vzryva)* 13 (4) (1977) 475.
[11] A.K. Lokenbakh, N.A. Zaporina, A.Z. Knipele, V.V. Strod, L.K. Lepin, *Combust. Explo. Shock Waves* 21 (1) (1985) 69–77.
[12] M.M. Mench, K.K. Kuo, C.L. Yeh, Y.C. Lu, *Combust. Sci. Technol.* 135 (1) (1998) 269–292.
[13] D.E. Jackson, D.F. Davidson, R.K. Hanson, in: *44th AIAA/ASME/SAE/ASEE Joint Propulsion Conference & Exhibit*, 2008, Paper No. AIAA-2008-4767.
[14] H. Tyagi, P.E. Phelan, R. Prasher, et al., *Nano Lett.* 8 (5) (2008) 1410–1416.
[15] J.M. Char, W.J. Liou, J.H. Yeh, C.L. Chiu, *Shock Waves* 6 (5) (1996) 259–266.
[16] K. Kumar, C.J. Sung, *Combust. Flame* 157 (4) (2010) 676–685.
[17] S.S. Vasu, D.F. Davidson, R.K. Hanson, *Combust. Flame* 152 (1–2) (2008) 125–143.
[18] G. Freeman, A.H. Lefebvre, *Combust. Flame* 58 (1984) 152–156.
[19] T. Edwards, L.Q. Maurice, *J. Propul. Power* 17 (2) (2001) 461–466.
[20] A. Violi, S. Yan, E.G. Eddings, et al., *Combust. Sci. Technol.* 174 (11) (2002) 399–417.
[21] W.S. Affleck, A. Thomas, *Proc. Inst. Mech. Eng.* 183 (1) (1969) 365–385.
[22] M.T. Donovan, X. He, B.T. Zigler, T.R. Palmer, M.S. Wooldridge, A. Atreya, *Combust. Flame* 137 (3) (2004) 351–365.
[23] G. Mittal, C.J. Sung, *Combust. Sci. Technol.* 179 (2007) 497–530.
[24] M. Ribaucour, R. Minetti, M. Carlier, L.R. Sochet, *J. Chim. Phys.* 89 (1992) 2121–2152.
[25] C.M. Allen, T. Lee, in: *47th AIAA Aerospace Sciences Meeting Including the New Horizons Forum and Aerospace Exposition*, 2009. Paper No. AIAA-2009-227.
[26] S. Tanaka, F. Ayala, J.C. Keck, *Combust. Flame* 133 (4) (2003) 467–481.
[27] J.A. Eastman, S.U.S. Choi, S. Li, W. Yu, L.J. Thompson, *Appl. Phys. Lett.* 78 (6) (2001) 718–720.
[28] A. Burcat, B. Ruscic, New NASA Thermodynamic Polynomials Database With Active Thermochemical Tables Updates. Report ANL 05/20 TAE 960. Available from: <ftp://ftp.technion.ac.il/pub/supported/aetdd/thermodynamics> (mirrored at 1.9.2010) <http://garfield.chem.elte.hu/Burcat/burcat.html> (mirrored at 1.9.2010).